Chemical Engineering Journal 165 (2010) 474–481

Contents lists available at ScienceDirect

Chemical Engineering Journal

journal homepage: www.elsevier.com/locate/cej

Preparation and characterization of baker's yeast modified by nano-Fe_3O_4: Application of biosorption of methyl violet in aqueous solution

Yu Tian [a], Chuyi Ji [a], Maojun Zhao [b], Meng Xu [b], Yunsong Zhang [b,*], Renguo Wang [b,*]

[a] College of Resource and Environment, Sichuan Agricultural University, Yaan 625014, PR China
[b] College of Life and Science, Sichuan Agricultural University, Yaan 625014, PR China

ARTICLE INFO

Article history:
Received 3 August 2010
Received in revised form
22 September 2010
Accepted 24 September 2010

Keywords:
Baker's yeast
Nano-Fe_3O_4
Magnetic
Glutaraldehyde
Methyl violet
Biosorption

ABSTRACT

The magnetic baker's yeast biomass (MB) was prepared by combining baker's yeast and nano-Fe_3O_4 using glutaraldehyde as a cross link agent. The MB was successfully used for the biosorption of methyl violet (MV) and was easily recycled by using an applied magnetic field. The mechanism of MV biosorption by MB was investigated by SEM, XRD, FTIR, zeta potential and potentiometric titration. The results revealed that nano-Fe_3O_4, with spherical and granular morphology, were distributed on the surface of baker's yeast biomass. The functional groups such as carboxyl, hydroxyl and amino groups found on the surface of MB may be responsible for MV biosorption. The optimal biosorption conditions were determined as pH 6.0, MV concentration 300 mg/L and contact time 30 min. The biosorption capacity in the optimal conditions was 60.84 mg/g. The biosorption process followed the pseudo-second-order kinetic model and the Langmuir isotherm equation. The thermodynamic parameters ΔG°, ΔH° and ΔS° showed that the biosorption was feasible, spontaneous and endothermic. The desorption and regeneration experiments were investigated and the biosorption/desorption cycles of MV were repeated three times. The MB regeneration efficiency and the MV recovery efficiency were 82.64% and 84.54% respectively in the third cycle by using HAc as an eluent solution.

1. Introduction

Synthetic dyes are widely used in a number of industrial processes, such as textile industries, paper printing and photography [1]. Dyes can have acute and chronic effects on organisms depending on the exposure time and dye concentrations. They also absorb and reflect sunlight and so can interfere with the growth of bacteria and hinder photosynthesis in aquatic plants [2,3]. Basic dyes have high brilliance and intensity of colors and are highly visible even in a very low concentration [4–6]. Methyl violet (MV), one of the triphenyl methane dyes which are more difficult to degrade than azo dyes as proved by Yuanlan Liu [7]. It is widely used in Gram staining and as an antiallergenic and as a bactericide, etc. For animals and humans, direct contact with MV can cause pain and congestion as well as irritating the respiratory tract and gastrointestinal systems [8]. At present, the dyeing industries waste water treatment techniques include physical, chemical and biological methods [9], in which the biological method has been highly valued over the world due to its effectiveness and high discoloration efficiency. Research in recent years has indicated that biosorption is one of the most promising technologies and the removal of dyes by different kinds of biosorbent materials has been receiving more attention [10,11].

As a cost-effective, easily available and safe industrial microorganism, yeast has been widely used in the study of biosorption of dyes and heavy metals [12,13]. Through investigating the adsorption mechanism of the saccharomyces cerevisiae towards pigment and optimizing the adsorption conditions, the technologies which isolate the dye from a large volume of polluted water are widely reported in the papers [14,15]. In these technologies centrifugation or filtration is one of the significant and necessary processes in the later part of separation. However, they are difficult for practical application due to their high costs and low efficiency. Furthermore, these methods may also result in secondary pollution. Therefore, isolation and recovery of biosorbent material becomes a limiting factor when considering the treatment of dyes by biosorption.

The magnetic separation technique has been shown to be a very promising method for solid–liquid phase separation. Nano-Fe_3O_4, which is super-paramagnetic, is used for purifying waste water from the dying industry and the removal of heavy metals according to the previous studies [16,17]. To use this characteristic in the recovery of biosorbent, magnetic baker's yeast biomass (MB) was made in our study. It could be a favorable biosorbent material for printing and dyeing waste water treatment. The new

* Corresponding authors. Tel.: +86 835 8563240; fax: +86 835 2862227.
E-mail addresses: yaanyunsong@yahoo.com.cn (Y. Zhang), wangrg60@163.com (R. Wang).

1385-8947/$ – see front matter © 2010 Elsevier B.V. All rights reserved.
doi:10.1016/j.cej.2010.09.037

material not only possesses the super-paramagnetic character of nano-Fe_3O_4, but also has the good biosorption capability of yeast which is advantageous for isolation and recovery.

In this work, the MB was prepared by joining baker's yeast biomass and nano-Fe_3O_4 using glutaraldehyde as cross link agent. Its biosorption potential was analyzed using MV as a model dye. The biosorption behavior of MB was examined by the Freundlich and Langmuir isotherm equations, as well as the pseudo-first-order and the pseudo-second-order kinetic models. Batch studies were carried out to identify the optimum biosorption conditions such as pH, equilibrium time, initial MV concentration and temperature. The MB characteristics and biosorption mechanism were examined by SEM, XRD, FTIR, zeta potential and potentiometric titration analysis. The desorption and regeneration experiments were also investigated.

2. Materials and methods

2.1. Preparation of MB

The baker's yeast was purchased from Harbin Mali Ltd., China. The samples were repeatedly washed with deionized water to remove adhering dirt and soluble impurities. They were then dried at 80 °C for 24 h and crushed and sieved to a particle size of under 100 meshes. The magnetic fluid (nano-Fe_3O_4) was prepared according to Shan Zhi's method [18]. 2.0 g of powdered biomass sample and magnetic fluid (the biomass/nano-Fe_3O_4 ratio used was 1:1) were suspended in 100 mL of 7% glutaradehyde solution. The mixture was stirred for 12 h at 25 °C and magnetically separated by an applied magnetic field. Then the sample was washed several times to remove the unreacted glutaradehyde. Finally, MB samples were prepared and stored at 4 °C in a refrigerator prior to biosorption studies.

2.2. MV solutions

The MV purchased from Tianjin Chemical Reagent No. 1 Plant, China, was selected as a representative reactive dye for this study. A stock solution of MV was prepared by dissolving 0.5 g of MV in 1 L of deionized water, and the concentrations of MV used (150–500 mg/L) were obtained by dilution of the stock solution. The pH of the solution was adjusted to the desired value by adding a small quantity of 0.1 mol/L HCl or 0.1 mol/L NaOH.

2.3. Biosorption studies

Batch biosorption studies were conducted in 150 mL conical flasks at different temperatures (25 °C, 35 °C, 45 °C and 55 °C). 30 mL of MV solution of initial concentration (150–500 mg/L) were stirred at 150 rpm in a rotary shaker (DH2-DA, China) with 0.50 g wet biosorbent dose (equal to 0.1050 g dry sample) for a required biosorption time (10–60 min). Varying pH of the solutions (3.0–9.0) was used. After that, the magnetic field was applied to separate the samples from the solution. The supernatants were analyzed to determine the concentration of the MV by spectrophotometer (WFJ-7200 Spectrophotometer, China) at λ_{max} of 578 nm. Biosorption capacity and the MV uptake efficiency were calculated using the following relationships:

$$q_t = \frac{(C_i - C_t)V}{m} \quad (1)$$

$$Q\,(\%) = \frac{C_i - C_t}{C_i} \times 100\% \quad (2)$$

where q_t is the amount of biosorption capacity at time t (mg/g), Q is the MV uptake efficiency, C_i is the initial concentration of MV (mg/L), C_t is the MV concentration at time t (mg/L), V is the volume of the solution (L) and m is the mass of the MB (g).

2.4. Desorption and regeneration studies

Desorption studies were carried out in 150 mL conical flasks. The MV-loaded biomass (MB) was magnetically separated. Then, the settled biomass was eluted with different eluents. The suspension was shaken at 150 rpm for 30 min to allow the MV to be released from the MB. The desorbed MV was analyzed and the MV recovery efficiency was calculated. Then the MB regeneration experiment was investigated and the MB regeneration efficiency was calculated as follows:

$$\text{Recovery efficiency} = \frac{\text{Amount of MV recovery}}{\text{Amount of MV biosorbed}} \times 100\% \quad (3)$$

$$\text{Regeneration efficiency} = \frac{\text{Regenerated adsorption capacity}}{\text{Original adsorption capacity}} \times 100\% \quad (4)$$

The following figure shows the synthesis route used to prepare MB and a suggested mechanism for MV biosorption/desorption onto MB.

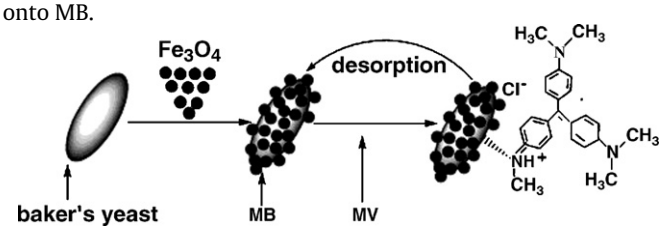

2.5. Characterization of MB

The surface structure and morphology of MB, yeast biomass and nano-Fe_3O_4 were characterized using a scanning electron microscope (JEOL JSM-5900LV, Japan) at a 20 kV acceleration voltage. Prior to analysis, the samples were coated with a thin layer of gold. The XRD pattern of nano-Fe_3O_4 and MB were obtained by a diffractometer (Holland Philip-X'Pert Pro) with Cu Kα radiation (λ = 1.5406 nm) in steps of 0.03° (2θ) min^{-1} from 15° to 75° (2θ). The zeta potential of MB, yeast biomass and nano-Fe_3O_4 were measured using zeta potential analyzer (Malvern-Zetasizer nano ZS UK) at pH 3–9. The type of binding groups present on the biosorbent were identified by Fourier transform infrared spectroscopy (Shimadzu FTIR-8400S, Japan) analysis in the region of 400–4000 cm^{-1} via the KBr pressed-disc method. The active sites present on the surface of MB were determined by potentiometric titration on autotitrator (ZD-2, China) with a combined glass electrode. The software ProtoFit Version 2.0 [19,20], a useful software tool for the calculation of pK_a values as well as surface site densities of biological material, was employed to fit acid–base titration data of the MB.

3. Results and discussion

3.1. Scanning electron microscope (SEM) analysis

The nano-Fe_3O_4, baker's yeast biomass and MB were analyzed by scanning electron microscopy to examine their surface structure and the results were given in Fig. 1. Fig. 1(a) shows that the nano-Fe_3O_4 had good dispersivity and regular particle size. Fig. 1(b) displays that the yeast cells were oval and their surfaces appeared to be smooth and even. Fig. 1(c) illustrates that MB surface was rather rough and some of the biomasses were clung together. It may be

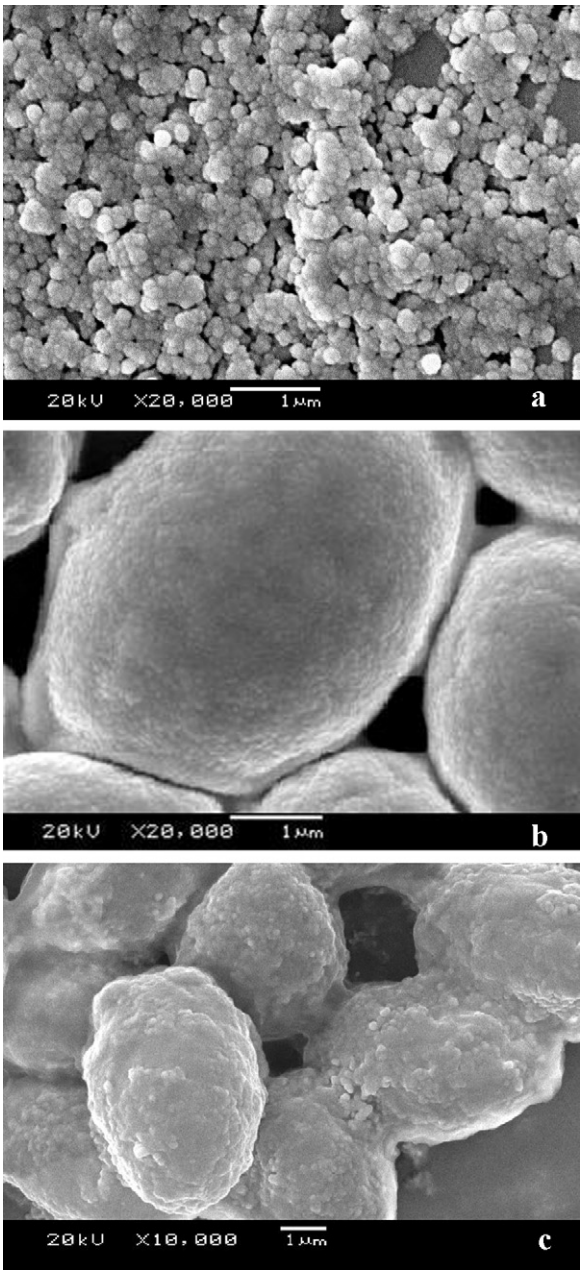

Fig. 1. SEM micrographs of nano-Fe_3O_4 (a), baker's yeast biomass (b) and MB (c).

attributed to the nano-Fe_3O_4 which adhered on baker's yeast surface, as well as the treatment of glutaraldehyde that made some biomass surfaces cross-linked.

3.2. XRD analysis and the amount of nano-Fe_3O_4 on MB

Fig. 2 shows the XRD patterns of nano-Fe_3O_4 and MB, the main crystal planes in a pure Fe_3O_4 crystals (2θ = 19.375, 30.535, 35.695, 43.315, 57.805 and 62.935), marked by their indices ((1 1 1), (2 2 0), (3 1 1), (4 0 0), (5 1 1), and (4 4 0)), were observed. The diffraction peaks of Fe_3O_4 match well with the inverse cubic spinel structure (JCPDS 19-0629). The XRD pattern of MB revealed the characteristic peaks of Fe_3O_4. It further confirms that the nano-Fe_3O_4 was loaded on yeast biomasses which contributed to the super-paramagnetic of MB. The peak intensity decreases and the full width of the peak increases, which indicates the low crystallinity and small crystallite size. It can be predominantly attributed to the existence of the

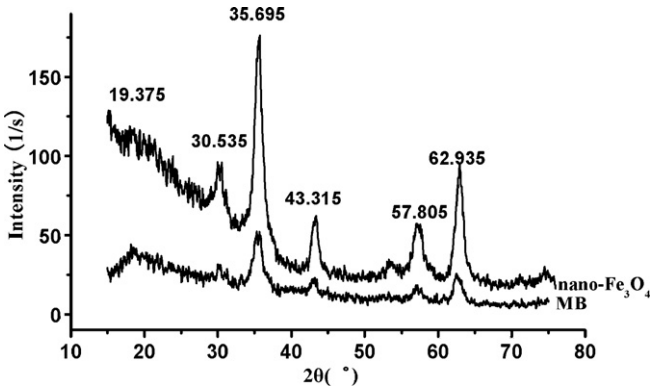

Fig. 2. X-ray diffraction spectra of nano-Fe_3O_4 and MB.

yeast biomass which affects the crystal size and crystallinity. The amount of nano-Fe_3O_4 on MB was measured with GB1868-1881-80 method [21] and was calculated as 0.3861 g/g. It reflected that a comparatively large amount of nano-Fe_3O_4 was on the MB surface, which posses a favorable superparamagnetism and is consistent with the results from SEM shown in Fig. 1(c).

3.3. Zeta potentials analysis

The surface charges of the baker's yeast biomass, nano-Fe_3O_4 and MB at the various pH values are shown in Fig. 3. Obviously, all the zeta potentials of the yeast biomass, nano-Fe_3O_4 and MB decreased with the increase in pH due to the deprotonation of the functional groups on the three materials. The pH_{PZC} of the yeast biomass and MB are about 4.5 and 4.7, respectively. However, for the nano-Fe_3O_4, the zeta potential is equal to 7.5. As presented in Fig. 3, the potential of the yeast biomass and the MB were equal at about pH 4.4. The lower positive charge of MB than that of baker's yeast biomass at pH < 4.4 resulted from less exposed organic functional groups on the surface of MB which attracted less H^+. It could be speculated that the nano-Fe_3O_4 was coated on MB to some degree and covered some of the functional groups on the yeast biomass. Moreover, that the yeast becomes more negatively charged than MB at pH > 4.7 further confirmed the attachment of nano-Fe_3O_4 onto the surface of the biomass. Nano-Fe_3O_4 combining with some of the functional groups on the surface of the biomass resulted in the amount of ionization of the functional

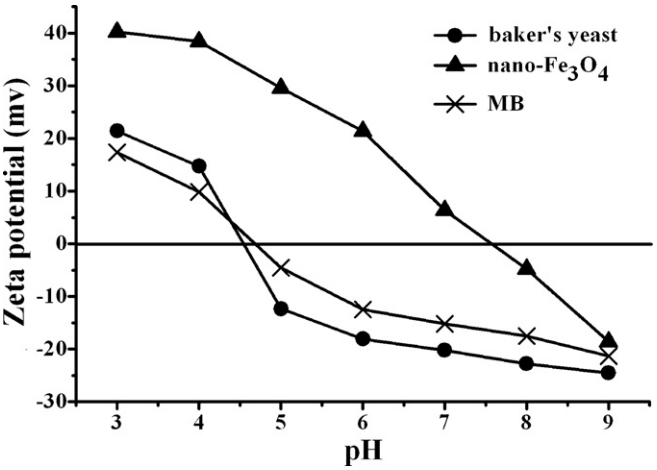

Fig. 3. Comparison of zeta potential of nano-Fe_3O_4, baker's yeast biomass and MB (nano-Fe_3O_4 concentration: 1.35 g/L; baker's yeast biomass concentration: 2.15 g/L; MB concentration: 3.5 g/L; contact time: 30 min; pH: 3–9).

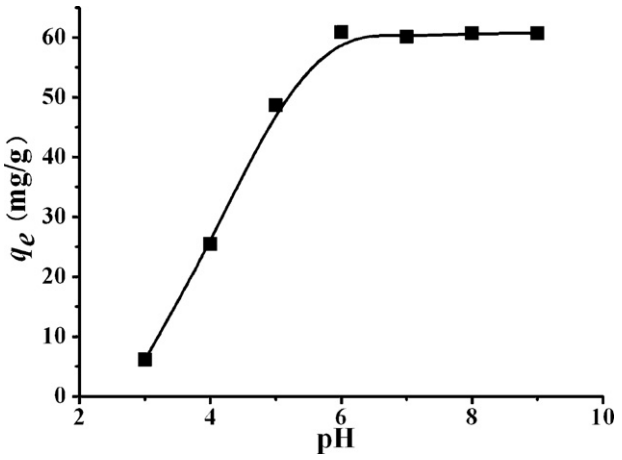

Fig. 4. Effect of pH on biosorption of MV (pH: 3–9; initial MV concentration: 300 mg/L; contact time: 30 min; biosorbent dosage: 3.5 g/L; temperature: 25 °C).

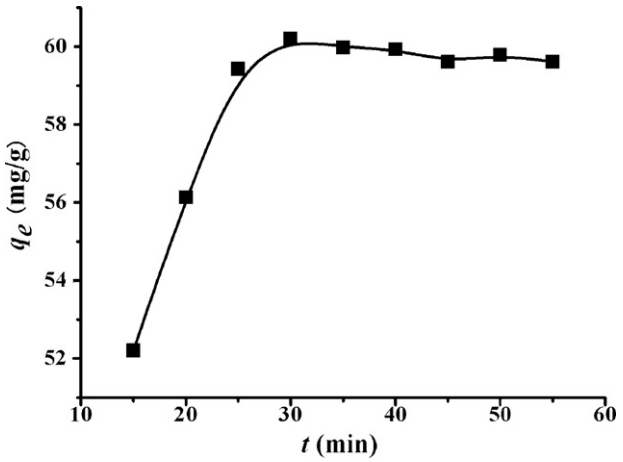

Fig. 5. Effect of contact time on biosorption of MV (pH: 6; initial MV concentration: 300 mg/L; biosorbent dosage: 3.5 g/L; temperature: 25 °C).

groups decreasing. Hence, the negative charge of the MB surface was less than that of baker's yeast.

3.4. Effect of pH on biosorption

Fig. 4 gives the biosorption capacity of MB within pH range 3.0–9.0. The uptake of MV increased with the increase in the solution pH and the maximum uptake of MV was observed as 60.84 mg/g, at pH 6.0. At low pH values, the poor biosorption of MV could be due to competition with the H^+ ions for binding sites on MB. Moreover, many protons will be available to protonate the MB surface in the condition, thereby the electrostatic repulsion between positively charged MV ions and positively charged biosorption sites causes the decrease in the dye biosorption. As the pH increased, the MB surface was more negatively charged and the functional groups (such as carboxyl, amino and hydroxyl groups) would be more deprotonated, thus attraction of MV ions was enhanced. From the zeta potential given in Fig. 3, the surface of MB was positively charged at pH < 4.7, not only the weak physical forces such as hydrogen bonding, van der Waals interactions but also the chemisorption might be involved in the biosorption process. At pH > 4.7, the surface of the biosorbent became negatively charged, the increased biosorption capacity was likely assigned to the electrostatic forces and the improvement of chemical action. At pH > 6 the negative charge on MB surface continues to increase with the rise of pH values, yet the biosorption capacity nearly remains constant. It reflects that the electrostatic attraction is not the only factor in the biosorption process. In the study, the MV at around pH 6 would be expected to interact most strongly with the negatively charged binding sites on the MB. As a result, the optimum pH for MV biosorption was found as 6 and the other biosorption experiments were performed at this pH value. In addition, the adaption of MB to pH values when above a certain value (pH > 6) was better compared with *Penicillium* sp. [22]. Similar results of the effect of pH were also reported by other researchers [23,24].

3.5. Effect of contact time

The effect of contact time on the biosorption of MV is depicted in Fig. 5. That the MV uptake increased rapidly over time illustrates the biosorption process was quite speedy, in respect that the abundant availability of binding sites present on the biomass surface as well as the biosorption of MV ions occurred on the surface of MB. The biosorption equilibrium was established within 30 min which was relatively a shorter time compared with other biosorbent [24]. At this point, the state of dynamic equilibrium was attained. Therefore, the optimum contact time was selected as 30 min for further experiments. Afterwards, the biosorption process more closely followed the time-dependent behavior. A moderately decreased biosorption capacity was also observed, by reason that some MV probably dropped off from the MB over time, the behavior illustrated that physical adsorption was possibly present in the process.

In order to analyze the biosorption kinetics of MV onto the MB, the pseudo-first-order and pseudo-second-order kinetics model were tested using the experimental data and rate constants in our study. The pseudo-first-order kinetic model and pseudo-second-order kinetic model were given in the following forms [25]:

$$\ln(q_e - q_t) = -k_1 t + \ln q_e \tag{5}$$

$$\frac{t}{q_t} = \frac{1}{k_2 q_e^2} + \frac{t}{q_e} \tag{6}$$

where q_e and q_t (mg/g) are the amounts of biosorption capacity at equilibrium and time t, respectively. k_1 is the rate constant of the pseudo-first-order equation (1/min). A plot of $\ln(q_e - q_t)$ versus t gives straight line and rate constant k_1 can be calculated from the slope (not shown). k_2 is the rate constant of the pseudo-second-order equation (g/(mg min). A plot of t/q_t versus t gives straight line and the values of k_2 can be calculated from the intercept of the plot (not shown).

As shown in Table 1, the correlation coefficient values (R^2) for pseudo-first-order kinetics are much lower than that for pseudo-second-order kinetics. The values of calculated biosorption capacity ($q_{e,cal}$) are near to experimental values ($q_{e,exp}$) for pseudo-second-order kinetics. Higher correlation coefficient values and similar $q_{e,cal}$ and $q_{e,exp}$ values revealed the better applicability of pseudo-second-order kinetics model. The results suggest that this biosorption involved a chemisorption process in addition to physisorption. The chemisorption might be the rate limiting step

Table 1
Comparison of the pseudo-first-order, pseudo-second-order biosorption rate constants and calculated and experimental q_e values.

$q_{e,exp}$ (mg/g)	Pseudo-first-order kinetic model			Pseudo-second-order kinetic model		
	k_1 (1/min)	R^2	$q_{e,cal}$ (mg/g)	k_2 (g/(mg min))	R^2	$q_{e,cal}$ (mg/g)
60.20	0.06429	0.5342	8.176	0.01050	0.9969	61.50

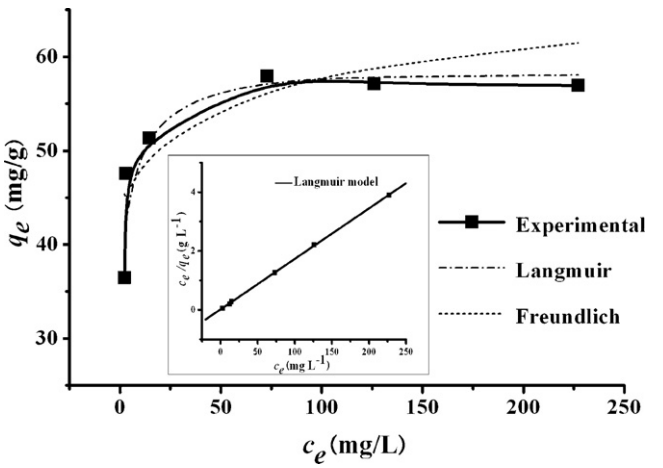

Fig. 6. Langmuir and Freundlich isotherms (initial MV concentration: 150–500 mg/L; pH: 6; contact time: 30 min; biosorbent dosage: 3.5 g/L; temperature: 25 °C).

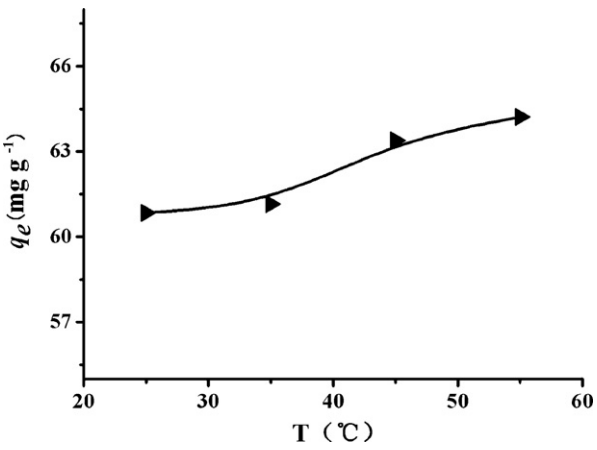

Fig. 7. Effect of temperature on the biosorption of MV (pH: 6; initial MV concentration: 300 mg/L; contact time: 30 min; biosorbent dosage: 3.5 g/L).

where valency forces are involved via electron sharing or exchange between the functional groups on MB and the MV ions [26].

3.6. Effect of the initial MV concentration and biosorption isotherms

The effect of MV concentration on the biosorption is given in Fig. 6. The data shows the biosorption capacity increased from 36.49 to 60.19 mg/g when MV concentration increased from 150 to 300 mg/L. It is attributed to the increase in driving force among MV ions at high initial concentration that enhanced effective collision probability between MV ions and MB. The biosorption capacity remained nearly constant in further increases in initial dye concentrations could be explained by the lack of sufficient surface area to accommodate more MV ions that are available in the solution. Similar findings have also been reported by other researchers [27,28]. These results suggest that the available sites on MB are the limiting factor for MV ions biosorption.

The equilibrium data was modeled with Langmuir and Freundlich isotherms. The purpose of the biosorption isotherms is to relate the adsorbate concentration of the bulk and the adsorbed amount at the interface [29]. The Langmuir adsorption isotherm has been successfully used to explain the adsorption of basic dyes from aqueous solutions [30–32]. The linear form of the Langmuir model is expressed as follows:

$$\frac{C_e}{q_e} = \frac{C_e}{qm} + \frac{1}{bq_m} \tag{7}$$

The Freundlich isotherm is an empirical equation assuming that the adsorption process takes place on heterogeneous surfaces and adsorption capacity is related to the concentration of dye at equilibrium [33]. A linear form of the Freundlich equation is given as:

$$\ln q_e = \frac{1}{n} \ln C_e + \ln k_F \tag{8}$$

where q_e and q_m are the equilibrium biosorption capacity and the maximum biosorption capacity of MB (mg/g). C_e is the equilibrium MV concentration in the solution (mg/L). b is the Langmuir adsorption equilibrium constant (L/mg) relating to the free energy and affinity of adsorption. k_F is a constant relating to the biosorption capacity and $1/n$ is an empirical parameter relating to the biosorption intensity, which varies with the heterogeneity of the materials.

As shown in Fig. 6, it was found that the data fitted better using Langmuir equation for MV biosorption, which revealed that the biosorption process was based on monolayer adsorption and was mostly on the surface-active areas of the MB. The Langmuir constant b, can be used to determine the suitability of the biosorbent for the sorbate using the Hall separation factor (R_L) as follows [34]:

$$R_L = \frac{1}{1 + bC_m} \tag{9}$$

where C_m is the highest initial MV concentration (mg/L). R_L is the constant separation factor (dimensionless) and can be used for interpretation of the sorption type as follows [35]:

$R_L > 1$ unfavorable
$R_L < 0$ unfavorable
$R_L = 1$ favorable (linear)
$0 < R_L < 1$ favorable
$R_L = 0$ irreversible

The value of R_L in the present investigation has been found to be 0.0021, indicating that the biosorption of MV on MB is favorable.

3.7. Effect of temperature and thermodynamic analysis

The biosorption process was studied while the reaction temperature was fixed at 25 °C, 35 °C, 45 °C and 55 °C, respectively. As shown in Fig. 7, the improvement in the biosorption capacity of MV with the increase in temperature reflects that the process is endothermic in nature [36]. The biosorption is favored by increased temperature. The reason for this behavior could be attributed to the increase in the mobility of MV ions with the increasing temperature and the amount of non-protonated functional groups on the MB increased due to the rise in the ionization constant of protonated functional groups over temperature. In addition, the increasing temperature may produce a swelling effect within the internal structure of the MB enabling MV ions to penetrate further. However, the temperature seems to have a relatively insignificant effect on MV biosorption by MB. It could be explained by the interactions of both electrostatic and chemical adsorptions. The electrostatic adsorption was an exothermic process, favoring low temperatures, while the rise of temperature was profitable for the chemical adsorption. That chemical and physical adsorption are occurring simultaneously in the biosorption process was consistent with the results from pH analysis.

Thermodynamic parameters are used to describe the thermodynamic behavior of the biosorption process. For such equilibrium reactions, K_c is the distribution constant which can be used to cal-

Table 2
Thermodynamic parameters for the biosorption of MV.

T (°C)	K_c (KJ/mol)	ΔG° (KJ/mol)	ΔH° (J/(mol K)	ΔS°
25	2.446	−2.220	5.824	26.83
35	2.489	−2.336		
45	2.839	−2.759		
55	2.986	−2.985		

culate the Gibbs free energy [37,38]:

$$K_c = \frac{C_{Ae}}{C_e} \quad (10)$$

$$\Delta G^\circ = -RT \ln K_c \quad (11)$$

$$\ln K_c = \frac{\Delta S\circ}{R} - \frac{\Delta H\circ}{RT} \quad (12)$$

where C_{Ae} (mg/L) is the amount adsorbed on solid at equilibrium and C_e (mg/L) is the equilibrium concentration of MV in the solution, respectively. R is the universal gas constant, 8.314 J/(mol K) and T is the absolute temperature (K). The ΔH° and ΔS° values were calculated from the slope and intercept of a Van't Hoff plot of $\ln K_D$ versus $1/T$ (not shown). Thermodynamic parameters are shown in Table 2.

The negative value of ΔG° at different temperatures reveals that the biosorption process was spontaneous in nature and the absolute value of ΔG° increased with the increase in temperature infers an enhancement of the spontaneity degree [39]. The change in the standard enthalpy (ΔH°) is 5.824 kJ/mol. The positive ΔH° value suggests the biosorption process is endothermic. The phenomenon indicates that chemisorption occurred between MB and MV. It is a chemisorption mechanism where there is an increase in the number of molecules acquiring sufficient energy to undergo chemical reaction with increasing temperature. The positive value of ΔS° shows an increased randomness in the solution during the biosorption process and suggests a good affinity of MV towards the biosorbent [40,41]. It was possibly due to the hydration shell on the MV surface, formed by numerous water molecules, was broken when the dye was biosorbed on MB, enabling most water molecules to enter the liquid phase.

3.8. Desorption and regeneration studies

To effectively make the biosorbent reusable in several biosorption/desorption cycles, desorption and regeneration experiments were carried out in our studies. The results at different eluent solutions of HAc (0.05 mol/L), HCl (0.001 mol/L), absolute ethanol as well as deionized water are shown in Table 3. The usage of the relatively low acid concentration was to avoid the hydrolysis of polysaccharide, destruction of steric configuration of protein in the yeast cell wall that might occur in a high acid concentration condition. In order to demonstrate the reusability of the MB, the biosorption/desorption (B/D) cycles of MV were repeated three times by using the same biosorbent (Table 3). It was found that the MB regeneration efficiency and the MV recovery efficiency using different eluents follow a decreasing order in general: HAc > HCl > absolute ethanol > deionized water. That the HAc solution was the most favorable eluent could be attributed to the organic acid characteristic. First, the eluent ionized H^+, which occupied the biosorption sites on MB surface thereby releasing MV ions. Second, there may be some remaining HAc on the surface of MB that increased the (COO^- content, which favors the regeneration efficiency in the recycling process. With regard to HCl, as an inorganic acid, on the basis of the theory of *similarity and intermiscibility*, was not as favorable as HAc probably due to lack of the solvent action towards MV. As for the elution condition in absolute ethanol, the MV was eluted through dissolution. Though the recovery efficiency is comparatively high, the enormous decline in the regeneration efficiency occurs in subsequent experiments. It is possibly assigned to the corrosion of the biomass surface by ethanol with osmosis and dehydration [42]. Table 3 also shows that some amounts of MV was desorbed with distilled water, it reflects that the physical adsorption, though relatively low, apparently existed in the removal process. The reasons for the decrease in regeneration efficiency were due to irreversible biosorption and the loss of MB in the process of reuse. Hence, from the analysis above, HAc solution was selected as the optimal eluent.

Table 3
Desorption and regeneration results by different eluents.

Eluents	Biosorption/desorption cycle	MB regeneration efficiency (%)	MV recovery efficiency (%)
HAc (0.05 mol/L)	1	97.84	89.31
	2	89.96	87.29
	3	82.64	84.54
HCl (0.001 mol/L)	1	72.59	68.45
	2	55.46	67.87
	3	45.43	65.41
Absolute ethanol	1	57.26	69.09
	2	23.67	67.34
	3	17.54	64.62
Distilled water	1	26.02	14.67
	2	18.92	13.85
	3	15.34	12.36

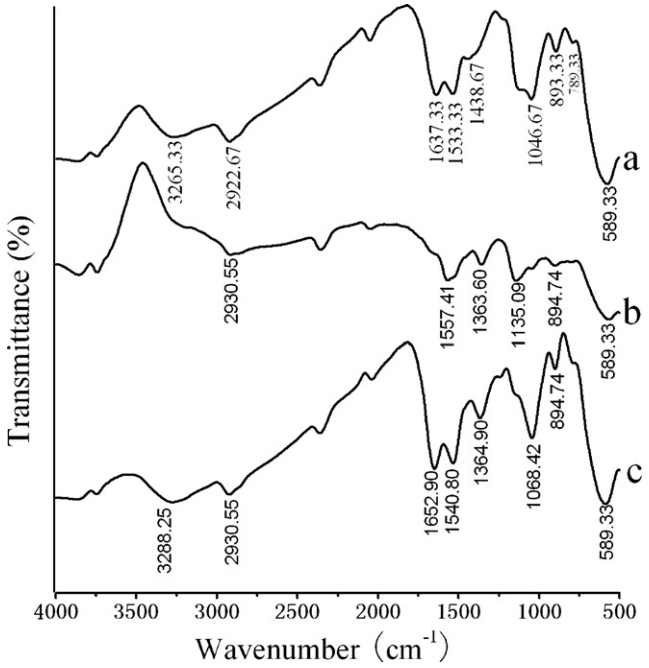

Fig. 8. FTIR spectra for MB (a), MB after biosorption (b) and MB after desorption (c).

3.9. FTIR analysis

In order to explain the biosorption mechanism of the MB, an FTIR study was carried out. The IR spectra of MB at different conditions are shown in Fig. 8. Fig. 8(a) displays that MB has a very complex structure and a number of absorption peaks. The peaks at 3265.33 cm^{-1} indicates the stretching band of –OH/(NH, while 2922.67 cm^{-1} belongs to the symmetrical stretching C(H of (CH_2 band. The peaks at 1637.33 cm^{-1} and 1533.33 cm^{-1} showed the stretching band of C=O from the amide I band and the bending band of N(H and C(N from the amide II band. They are the characteristic absorption peaks of protein. The vibrating absorption

Table 4
Concentration and acidity constants for surface functional groups of MB (MB: 3 g/L; titrant: 0.1 mol/L NaOH; reaction temperature: 25 ± 0.5 °C; background electrolyte: 0.1 mol/L NaCl).

Biosorbent	Functional group	pK_a value reported	pK_a value obtained	Site density (mmol/g)
MB	Carboxyl	2.0(6.0	4.02(5.90	0.35 ± 0.06
	Phosphoryl	0.2(2.9/5.6(7.2	6.00(7.13	0.28 ± 0.02
	Amine	9.0(11.0	9.39(9.46	0.12 ± 0.07
	Hydroxyl	8.0(12	8.36(9.71	0.31 ± 0.09

peak at 1438.67 cm^{-1} was from the asymmetric C(H bending of (CH_3 or the stretching band of C(OH from the uronic acid. The peak at 1046.67 cm^{-1} probably comes from both the stretching band of C(N from the amide III and the stretching band of P(O(C. Hence an inference can be drawn that the active groups such as (OH/(NH, C═O, (COOH, P(O(C, most of which were the characteristic groups of protein and carbohydrate [43], were located on the surface of MB. An evident peak at 589.33 cm^{-1} with respect to the characteristic groups of nano-Fe_3O_4 further confirmed the loading of nano-Fe_3O_4 onto the biomass surface. Fig. 8(b) shows the MB loaded with MV. The peaks at 3265.33 cm^{-1} attributed to –NH/–OH absorbance disappeared. This means that –NH/–OH participated in the adsorption processes of MV. Moreover, the adsorption peak at 1637.33 cm^{-1} almost disappeared and the strength of adsorption peak at 1533.33 cm^{-1} significantly decreased. These phenomena reflect the involvement of C═O and N(H in biosorption. An evident change of C(OH absorption peaks at 1438.67 cm^{-1} infers that (COOH on the surface of MB contributed to the biosorption as well. The strengthening of C(H asymmetric vibration peaks of (CH_3 at 1363.60 cm^{-1} may be attributed to biosorption of MV onto MB. The spectrum of MB after desorption is given in Fig. 8(c). The absorption bands represent the adsorptive groups which are similar to that in Fig. 8(a). It could have resulted from the use of HAc, which exposed those organic groups by dropping MV off from the surface of MB during the eluting process. The acid that remained on the surface of the biosorbent may have increased the (COOH content of MB which contributed to the strengthened peak at around 1364.90 cm^{-1}. To sum up, the changes observed in the FTIR spectra mentioned above revealed that the HAc had a favorable desorption effect on MB. It could also be confirmed that the functional groups such as (OH/(NH, (COOH and (CONH(were likely responsible for MV biosorption.

3.10. Determination of active sites

The study of the proton binding active zone of biosorbent is of great importance [19,44]. Fig. 9 depicts a comparison of titration curves of the MB and the 0.1 mol/L NaCl electrolyte. It is evident from the figure that the MB provided significant buffering capacity to the solution across the pH range studied comparing with the blank (no MB). The substantial capacity is due to functional groups on the biomass surface consuming the added base by donating protons. The pK_a values of organic functional groups and the corresponding site densities c_{Ai} were calculated by using the software ProtoFit [44]. By combining the microorganism cell wall structure and comparisons of prior literature report [44,45], it is suggested that the carboxyl, amino, hydroxyl and phosphoryl groups mainly presented on yeast biomass. Analysis of the titration data indicates that a four-site model provides good fit for the MB. The acidity constants and site concentrations for each type of surface functional groups on MB are summarized in Table 4. It shows that carboxyl, amine, hydroxyl and phosphoryl groups were all present on the MB surface. Those groups showed lower concentrations with different degrees compared to our previous study [42], it was possibly attributed to the cross linking reaction with glutaraldehyde, and the biomass was coated by nano-Fe_3O_4. According to the potentiometric titration results, it is suggested that the carboxyl, amine, hydroxyl and phosphoryl groups mainly present on MB, which are responsible for MV biosorption, the outcome verifies the results of previous IR.

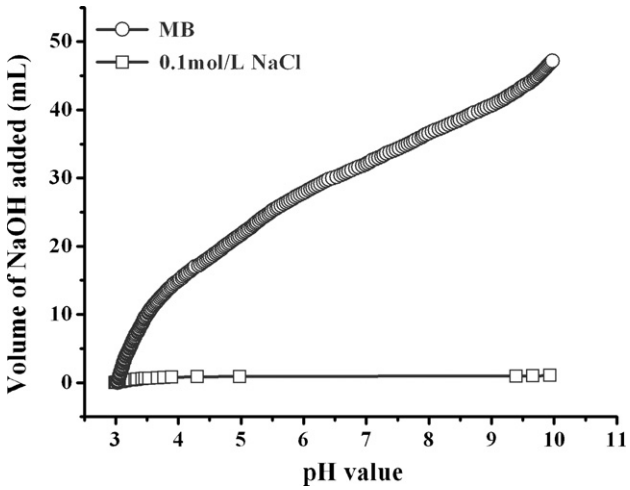

Fig. 9. The titration curve of the MB (MB: 3 g/L; itrant: 0.1 mol/L NaOH; reaction temperature: 25 ± 0.5 °C; background electrolyte: 0.1 mol/L NaCl).

4. Conclusions

MB, as a potential reusable dye biosorbent, was prepared by baker's yeast and nano-Fe_3O_4. It could be recycled easily by an applied magnetic field and regenerated for reusing. The MV biosorption properties of MB were investigated in our study. Results showed that MB was an effective biosorbent for biosorption of MV from an aqueous solution. The functional groups such as carboxyl, hydroxyl and amine on the MB surface were found responsible for MV biosorption. The optimum biosorption conditions were determined as pH 6.0, initial MV concentration 300 mg/L and contact time 30 min. The kinetic and equilibrium data were explained adequately by the pseudo-second-order kinetic model and the Langmuir isotherm model, respectively. The thermodynamic results revealed the feasibility, endothermic and spontaneous nature of the biosorption. Regeneration studies presented that the HAc solution (0.05 mol/L) is the optimal eluent and confirmed that MB could be effectively utilized for the removal of MV after recycling. Hence, MB is a potentially recyclable biosorbent for the water-soluble dye disposals that is effective and easily regenerated.

Acknowledgments

This research was supported by the Key Basic Research Program of the Sichuan Provincial Education Commission, PR China (Grant Nos. 07ZA063, 2005A014). Sincere thanks go to Mr Lawrence Gray for providing language assistance, and to anonymous reviewers for helpful suggestions.

References

[1] D.A. Oxspring, G. McMullan, W.F. Smyth, R. Marchant, Decolourisation and metabolism of the reactive textile dye, Remazol Black B, by an immobilized microbial consortium, Biotechnol. Lett. 18 (1996) 527–530.
[2] I.M. Robinson, G. McMullan, R. Marchant, P. Nigam, Remediation of dyes in textile effluent: a critical review on current treatment technologies, Bioresour. Technol. 77 (2001) 247–255.
[3] Y.M. Slokar, A.M. Le Marechal, Methods of decoloration of textile waste waters, Dyes Pigment 37 (1998) 335–356.
[4] E.A. Clarke, R. Anliker, Organic dyes and pigments, Handb. Environ. Chem. Anthropogenic Compd. A 3 (1980) 181–215.
[5] I.M. Banat, P. Nigam, D. Singh, R. Marchant, Microbial decolourization of textile-dye containing effluents: a review, Bioresour. Technol. 58 (1996) 217–227.
[6] Y. Fu, T. Viraraghavan, Fungal decolourization of wastewaters: a review, Bioresour. Technol. 79 (2001) 251–262.
[7] Y.L.Liu, Y.F.Du, J.X.Lu, Chinese Shanghai Environ Sci [J]. 22 (2003) 888 (in Chinese).
[8] http://www.chemicon.com/webfiles/MSDS/ECM508MSDS.pdf, Material Safety Data Sheet.
[9] E. Forgacs, T. Cserhatia, G. Oros, Removal of synthetic dyes from waste waters: a review, Environ. Int. 30 (2004) 953–971.
[10] O. Anjaneya, M. Santoshkumar, S.N. Anand, T.B. Karegoudar, Biosorption of acid violet dye from aqueous solutions using native biomass of a new isolate of *Penicillium* sp., Int. Biodeter. Biodegrad. 63 (2009) 782–787.
[11] R. Aravindhan, J.R. Rao, B.U. Nair, Removal of basic yellow dye from aqueous solution by sorption on green alga *Caulerpa scalpelliformis*, J. Hazard. Mater. 142 (2007) 68–76.
[12] T. Akar, A.S. Ozcan, S. Tunali, A. Ozcan, Biosorption of a textile dye (Acid Blue 40) by cone biomass of Thuja orientalis: estimation of equilibrium, thermodynamic and kinetic parameters, Bioresour. Technol. 99 (2008) 3057–3065.
[13] S.B. Deng, Y.P. Ting, Characterization of PEI-modified biomass and biosorption of Cu(II), Pb(II) and Ni(II), Water Res. 39 (2005) 2167–2177.
[14] I. Šafařik, L. Ptáčková, M. Šafařiková, Adsorption of dyeson magnetically labeled baker's yeast cells, Eur. Cell Mater. 3 (2002) 52–55.
[15] Z. Aksu, Reactive dye bioaccumulation by *Saccharomyces cerevisiae*, Process Biochem. 38 (2003) 1437–1444.
[16] Y.F. Shen, J. Tanga, Z.H. Nie, Y.D. Wang, Y. Ren, L. Zuo, Preparation and application of magnetic Fe_3O_4 nanoparticles for waste water purification, Sep. Purif. Technol. 68 (2009) 312–319.
[17] Y.C. Chang, D.H. Chen, Preparation and adsorption properties of monodisperse chitosan-bound Fe_3O_4 magnetic nanoparticles for removal of Cu(II) ions, J. Colloid Interface. Sci. 283 (2005) 446–451.
[18] X.X. Wang, S. Huang, Z. Shan, Preparation of Fe_3O_4@Au nano-composites by self-assembly technique for immobilization of glucose oxidase, Chin. Sci. Bull. 54 (2009) 1176–1181.
[19] S.Q. Memon, N. Memon, S.W. Shah, M.Y. Khuhawar, M.I. Bhanger, Sawdust – a green and economical sorbent for the removal of cadmium(II) ions, J. Hazard. Mater. 139 (2007) 116–121.
[20] P. Lodeiro, A. Fuentes, R. Herrero, D.E. Sastre, M.E. Vicente, Cr(III) binding by surface polymers in natural biomass: the role of carboxylic groups, Environ. Chem. 5 (2008) 355–365.
[21] X. Pan, Continuous analysis of Fe, Al in phosphate rock by colorimetric method, Phosphate Compd. Fert. 06 (1999) 62–63 (in Chinese).
[22] O. Anjaneya, M. Santoshkumar, S. Nayak Anand, T.B. Karegoudar, Biosorption of acid violet dye from aqueous solutions using native biomass of a new isolate of *Penicillium* sp., Int. Biodeter. Biodegr. 63 (2009) 782–787.
[23] B.H. Hameed, Equilibrium and kinetic studies of methyl violet sorption by agricultural waste, J. Hazard. Mater. 154 (2008) 204–212.
[24] L. Ping, Y.J. Su, Y. Wang, B. Liu, L.M. Sun, Bioadsorption of methyl violet from aqueous solution onto Pu-erh tea powder, J. Hazard. Mater. 179 (2010) 43–48.
[25] Y.S. Ho, G. McKay, Pseudo-second order model for sorption processes, Process. Biochem. 34 (1999) 451–465.
[26] S.R. Shukla, R.S. Pai, Adsorption of Cu(II), Ni(II) and Zn(II) on dye loaded groundnut shells and sawdust, Sep. Purif. Technol. 43 (2005) 1–8.
[27] A. Özer, A. Gönül, M. Turabik, The biosorption of Acid Red 337 and Acid Blue 324 on Enteromorpha prolifera: the application of nonlinear regression analysis to dye biosorption, Chem. Eng. J. 112 (2005) 181–190.
[28] C. Ferdağ, N. olaka, A. Atarb, Olgunb, Biosorption of acidic dyes from aqueous solution by *Paenibacillus macerans*: kinetic, thermodynamic and equilibrium studies, Chem. Eng. J. 150 (2009) 122–130.
[29] J. Eastoe, J.S. Dalton, Dynamic surface tension and adsorption mechanisms of surfactants at the air–water interface, Adv. Colloid Interface. Sci. 85 (2000) 103–144.
[30] B.H. Hameed, A.T.M. Din, A.L. Ahmad, Adsorption of methylene blue onto bamboo-based activated carbon: kinetics and equilibrium studies, J. Hazard. Mater. 141 (2007) 819–825.
[31] I.A.W. Tan, B.H. Hameed, A.L. Ahmad, Equilibrium and kinetic studies on basic dye adsorption by oil palm fibre activated carbon, Chem. Eng. J. 127 (2007) 111–119.
[32] B.H. Hameed, A.L. Ahmad, K.N.A. Latiff, Adsorption of basic dye (methylene blue) onto activated carbon prepared from rattan sawdust, Dyes Pigment 75 (2007) 143–149.
[33] S. Karaca, A. Gürses, M. Açıkyıldız, M. Ejder, Adsorption of cationic dye from aqueous solutions by activated carbon, Micropor. Mesopor. Mater. 115 (2008) 376–382.
[34] R. Nadeem, M.A. Hanif, F. Shaheen, S. Perveen, M.N. Zafar, T. Iqbal, Physical and chemical modification of distillery sludge for Pb(II) biosorption, J. Hazard. Mater. 150 (2008) 335–342.
[35] S. Dahiya, R.M. Tripathi, A.G. Hegde, Biosorption of heavy metals and radionuclide from aqueous solutions by pre-treated arca shell biomass, J. Hazard. Mater. 150 (2008) 376–386.
[36] A.E. Ofomaja, Y.S. Ho, Effect of temperature and pH on methyl violet biosorption by Mansonia wood sawdust, Bioresour. Technol. 99 (2008) 5411–5417.
[37] V. Padmavathy, Biosorption of nickel(II) ions by baker's yeast: kinetic, thermodynamic and desorption studies, Bioresour. Technol. 99 (2008) 3100–3109.
[38] L. Abramian, H. El-Rassy, Adsorption kinetics and thermodynamics of azo-dye Orange II onto highly porous titania aerogel, Chem. Eng. J. 150 (2009) 403–410.
[39] X.F. Sun, S.G. Wang, X.W. Liu, W.X. Gong, N. Bao, B.Y. Gao, H.Y. Zhang, Biosorption of Malachite Green from aqueous solutions onto aerobic granules: kinetic and equilibrium studies, Bioresour. Technol. 99 (2008) 3475–3483.
[40] A. Kilislioglu, B. Bilgin, Thermodynamic and kinetic investigations of uranium adsorption on Amberlite IR-118H resin, Appl. Radiat. Isot. 58 (2003) 155–160.
[41] S.W. Won, K. Hyun-Jong, C. Soo-Hyung, C. Bong-Woo, K. Ki-Ju, Y. Yeoung-Sang, Performance, kinetics and equilibrium in biosorption of anionic dye reactive Black 5 by the waste biomass of *Corynebacterium glutamicum* as a low-cost biosorbent, Chem. Eng. J. 121 (2006) 37–43.
[42] Y.S. Zhang, W.G. Liu, M. Xu, F. Zheng, M.J. Zhao, Study of the mechanisms of Cu^{2+} biosorption by ethanol/caustic-pretreated baker's yeast biomass, J. Hazard. Mater. 178 (2010) 1085–1093.
[43] J.X. Yu, M. Tong, X.M. Sun, B.H. Li, Enhanced, selective adsorption of Pb^{2+} and Cu^{2+} by EDTAD-modified biomass of baker's yeast, Bioresour. Technol. 99 (2008) 2588–2593.
[44] B. Astrid, M. Henry, B. Gert, Interaction of uranium(VI) with lipopolysaccharide, Dalton T (2008) 2879–2886.
[45] Y. Nathan, L.G. Benning, V.R. Phoenix, F.G. Ferris, Characterization of metal-cyanobacteria sorption reactions: A combined macroscopic and infrared spectroscopic investigation, Environ. Sci. Technol. 38 (2004) 775–782.